Nuclear Science and Techniques (2025) 36:44
https://doi.org/10.1007/s41365-024-01612-0

Production of unknown neutron-deficient isotopes with $Z = 99–106$ in multinucleon transfer reaction $^{124}Xe+^{249}Cf$

Na Tang[1,2] · Si-Ying Ma[1] · Rong An[1,2] · Jing-Jing Li[3] · Feng-Shou Zhang[2,4,5]

Received: 27 August 2024 / Revised: 29 September 2024 / Accepted: 9 October 2024 / Published online: 28 January 2025

Abstract

The dinuclear system approach, coupled with the statistical decay model GEMINI++, was used to investigate multinucleon transfer reactions. Experimental production cross-sections in the reaction $^{129}Xe+^{248}Cm$ were reproduced to assess the reliability of these theoretical models. The production of neutron-deficient transcalifornium nuclei with $Z = 99 - 106$ was examined in multinucleon transfer reactions, including $^{124}Xe + ^{248}Cm$, $^{124}Xe + ^{249}Cf$, and $^{129}Xe+ ^{249}Cf$. Both the driving potential and the neutron-to-proton equilibration ratio were found to dominate the nucleon transfer process. The reaction $^{124}Xe + ^{249}Cf$ is proposed as a promising projectile-target combination for producing neutron-deficient isotopes with $Z = 99 - 106$, with the optimal incident energy identified as $E_{c.\,m.} = 533.64$ MeV. Production cross-sections of 25 unknown neutron-deficient trancalifornium isotopes with cross-sections greater than 1 pb were predicted.

Keywords Multinucleon transfer reaction · Dinuclear system · Unknown neutron-deficient isotopes with $Z = 99–106$

1 Introduction

The synthesis of heavy and super-heavy nuclei (SHN) has drawn considerable interest in nuclear physics [1–6]. Notably, nuclei with N=184 and Z=114 are predicted double magic nuclei at the center of the island of stability [7], which also is predicted by early calculations. Up to now, this landscape of nuclear charts now includes elements up to Z= 118 element. Fusion-evaporation reaction, particularly effective for neutron-deficient nuclei, has become a crucial method for producing heavy and SHN [8–11]. For instance, such as ^{262}Bh, ^{265}Hs, ^{267}Mt, ^{269}Ds, and ^{272}Rg have been synthesized using ^{208}Pb and ^{209}Bi targets [12–16]. Over recent decades, ongoing research to produce neutron-deficient actinide nuclei has been carried out at facilities including Lawrence Berkeley National Laboratory (LBNL, Berkeley) [17], Flerov Laboratory of Nuclear Reactions (FLNR, Dubna) [18], and the Institute of Modern Physics (IMP, Lanzhou) [9, 19, 20]. Recently, ^{249}No was detected via the α-decay of the new isotope ^{253}Rf [21]. Although fusion-evaporation reactions continue to be a promising approach for synthesizing neutron-deficient nuclei in the heavy-mass region [22, 23], the resulting mass spectrum remains relatively narrow. The multinucleon transfer (MNT) reaction, characterized by its wide mass range due to broad excitation functions within the

This work was supported partly by the National Key R&D Program of China (No. 2023YFA1606401) and the National Natural Science Foundation of China (Nos. 12135004, 11635003, 11961141004, 12105019, and 12047513), the Open Project of Guangxi Key Laboratory of Nuclear Physics and Nuclear Technology (No. NLK2023-05), and the Central Government Guidance Funds for Local Scientific and Technological Development, China (No. Guike ZY22096024).

✉ Feng-Shou Zhang
fszhang@bnu.edu.cn

[1] School of Physics, Ningxia University, Yinchuan 750021, China

[2] School of Physics and Astromony, College of Nuclear Science and Technology, Beijing Normal University, Beijing 100875, China

[3] College of Material Science and Technology, Nanjing University of Aeronautics and Astronautics, Nanjing 210016, China

[4] Key Laboratory of Beam Technology of Ministry of Education, Institute of Radiation Technology, Beijing Academy of Science and Technology, Beijing 100875, China

[5] Center of Theoretical Nuclear Physics, National Laboratory of Heavy Ion Accelerator of Lanzhou, Lanzhou 730000, China

transfer process, offers an alternative approach for extending the nuclear chart landscape [24–27].

Since the 1970s, transfer reactions and deep inelastic heavy-ion collisions have been extensively studied, resulting in the identification of new neutron-deficient actinide nuclei and neutron-rich isotopes of light nuclei [28–34]. The products of MNT reactions are closely related to the structure of the reaction system and the projectile-target mass asymmetry [35–37]. Typically, neutron-deficient beams paired with actinide targets are used to produce neutron-deficient actinide isotopes through MNT reactions. For instance, five new neutron-deficient isotopes, ^{216}U, ^{219}Np, ^{223}Am, ^{229}Am, and ^{233}Bk, were identified in the reaction ^{48}Ca +^{248}Cm [38]. Recently, a new isotope, ^{241}U, was synthesized, and systematic atomic mass measurements of 19 neutron-rich Pa-Pu isotopes were conducted using the MNT reaction of the ^{238}U+^{198}Pt system at the KISS facility [39]. Consequently, the MNT reaction mechanism provides an accessible pathway to synthesize previously unknown actinide nuclei.

Various theoretical techniques have been developed to describe transfer reactions in low-energy heavy-ion collisions. These include semi-classical models such as the Grazing model [40, 41], Grazing-F model [42], the dinuclear system (DNS) model [5, 37, 43–50], the dynamical model based on multidimensional Langevin equations [51–56], the improved quantum molecular dynamics (ImQMD) model [57–61], and the time-dependent Hartree–Fock (TDHF) approach [62, 63, 63, 64]. These models have enabled extensive investigation of topics such as the production cross-sections of new isotopes [65], shell effect on fragment formation [66], total kinetic energy spectra of transfer fragments [60], and angle distributions for MNT products [67]. Notably, MNT reactions reveal unique features, including the ability to manually control nucleon transfer, the interaction mechanisms of projectile-target combinations, and the impact of incident energy on the production cross-sections of neutron-deficient actinide nuclei in theoretical studies.

Due to isospin relaxation, MNT reactions using neutron-deficient beams offer advantages in accessing neutron-deficient isotopes within the actinide region [68]. The properties of these neutron-deficient heavy isotopes are essential for investigating shell evolution and proton driplines. In addition to fusion-evaporation reactions, MNT reactions may present a viable pathway for producing neutron-deficient heavy isotopes [68]. The primary goal of studying MNT reactions with actinide targets is to probe an island of stability. This study focuses on the production of unknown neutron-deficient isotopes with $Z = 99 - 106$ using the DNS model via ^{124}Xe+^{248}Cm, ^{124}Xe+^{249}Cf, and ^{129}Xe+^{249}Cf reaction systems. The de-excitation process is addressed using the GEMINI++ statistical model.

The remainder of this paper is organized as follows. In Sect. 2, we provide a brief overview of the theoretical framework of the DNS model. The results and discussion are presented in Sect. 3. Finally, a summary and outlook are presented in Sect. 4.

2 Theoretical framework

The DNS model describes a diffusion process that takes place along the relative distance between the centers of interacting nuclei and in terms of mass asymmetry. The probability $P(Z_1, N_1, E_1, t)$ for the mass distribution of a fragment with proton number Z_1 and neutron number N_1 can be determined by solving the master equation [69].

$$\begin{aligned}\frac{\mathrm{d}P(Z_1,N_1,E_1,t)}{\mathrm{d}t} &= \sum_{Z_1'} W_{Z_1,N_1;Z_1',N_1}(t) \\ &\Big[\mathrm{d}_{Z_1,N_1}P(Z_1',N_1,E_1',t) \;-\mathrm{d}_{Z_1',N_1}P(Z_1,N_1,E_1,t)\Big] \\ &+\sum_{N_1'} W_{Z_1,N_1;Z_1,N_1'}(t) \\ &\Big[\mathrm{d}_{Z_1,N_1}P(Z_1,N_1',E_1',t) \;-\mathrm{d}_{Z_1,N_1'}P(Z_1,N_1,E_1,t)\Big],\end{aligned} \tag{1}$$

where $W_{Z_1,N_1;Z_1',N_1}(t)$ and $W_{Z_1,N_1;Z_1,N_1'}(t)$ are the mean transition probabilities from channel (Z_1, N_1) to (Z_1', N_1) and (Z_1, N_1) to (Z_1, N_1') at the time t, respectively. The quantity d_{Z_1,N_1} denotes the microscopic dimension, that is, the microscopic state number of the fragment for the macroscopic state (Z_1, N_1, E_1) [70]. The locally excited energy E_1 of the composite system is provided by the dissipation of the relative kinetic energy. The relationship between the transition probability and local excitation energy can be expressed as follows:

$$\begin{aligned}&W_{Z_1,N_1;Z_1',N_1}(t) \\ &= \frac{\tau_{\mathrm{mem}}\left[Z_1,N_1,E_1\left(Z_1,N_1\right);Z_1',N_1,E_1\left(Z_1',N_1\right)\right]}{\mathrm{d}_{Z_1,N_1}\mathrm{d}_{Z_1',N_1}\hbar^2} \\ &\times\sum_{ii'}\left|\left\langle Z_1',N_1,E_1\left(Z_1',N_1\right),i'|V(t)|Z_1,N_1,E_1\left(Z_1,N_1\right),i\right\rangle\right|^2.\end{aligned} \tag{2}$$

where i denotes the remaining quantum numbers. During the diffusion process, a single-nucleon transfer at each time step was assumed in DNS model as follows: $Z_1' = Z_1 \pm 1$ or $N_1' = N_1 \pm 1$. Memory time τ_{mem} is expressed as

$$\tau_{\mathrm{mem}}\left(Z_1,N_1,E_1;Z_1',N_1,E_1';t\right) = \hbar\left[\frac{2\pi}{\sum_{KK'}\left\langle V_{KK'}V_{KK'}^*\right\rangle}\right]^{1/2}. \tag{3}$$

More details regarding the memory time τ_{mem} are discussed in Ref. [71]. The excitation energy in the DNS model can be expressed as follows:

$$E_1(Z_1,N_1) = E_{\rm diss} - \left[U\left(Z_1,N_1,Z_2,N_2\right) - U\left(Z_P,N_P,Z_T,N_T\right)\right] - \frac{M^2}{2\zeta_{\rm int}}, \tag{4}$$

where $E_{\rm diss}$ is the energy dissipated into the composite system and is associated with the incident energy and entrance angular momentum J [72]. M and $\zeta_{\rm int}$ denote the intrinsic angular momentum of the DNS and intrinsic moment of inertia, respectively [72]. The fragment distributions are strongly influenced by $E_{\rm diss}$

$$E_{\rm diss}(t) = E_{\rm c.m.} - V_{\rm cont}\left(Z_{\rm p},N_{\rm p},R_{\rm cont}\right) - \frac{\langle J(t)\rangle^2}{2\zeta_{\rm rel}} - \langle E_{\rm rad}(J,t)\rangle. \tag{5}$$

The dissipation of the relative angular momentum$\langle J(t)\rangle$ can be calculated as $\langle J(t)\rangle = J_{\rm st} + (J - J_{\rm st})\exp[-t/\tau_J)]$, where the angular momentum the relaxation time $\tau_J = 12\times10^{-22}$ s. $J_{\rm st}$ denotes angular momentum at the stick limit. The radial energy at time t is given by $\langle E_{\rm rad}(J,t)\rangle = E_{\rm rad}(J,0)\exp(-t/\tau_R)$, where τ_R ($\tau_R = 2\times10^{-22}$ s) is the relaxation time of the radial kinetic energy [73].

The potential energy surface (PES) of a projectile-target system is critical in governing the nucleon transfer process [74, 75], which can be expressed as follows:

$$U\left(Z_1,N_1,R_{\rm cont}\right) = \Delta\left(Z_1,N_1\right) + \Delta\left(Z_2,N_2\right) + V_{\rm cont}\left(Z_1,N_1,R_{\rm cont}\right). \tag{6}$$

where $\Delta(Z_1,N_1)$ and $\Delta(Z_2,N_2)$ are the mass excesses of fragments (Z_1,N_1) and (Z_2,N_2), respectively. $V_{\rm cont}(Z_1,N_1,R_{\rm cont})$ is the effective nucleus-nucleus interaction potential for the two fragments, and $R_{\rm cont}$ is the location of the potential pocket if the nucleus–nucleus potential contains a potential pocket [73]. The position at which the nucleon transfer process occurs for the reaction without potential pockets can be obtained using the equation $R_{\rm cont} = R_1\left[1+\beta_2^{(1)}Y_{20}(\theta_1)\right] + R_2[1+\beta_2^{(2)}Y_{20}(\theta_2)\Big] + 0.7$ fm [69]. Here, $R_{1,2} = 1.16\,A_{1,2}^{1/3}$ fm and $\beta_2^{(i)}$ ($i = 1, 2$) is the quadrupole deformation parameter of fragment i which can be obtained from Ref. [76].

The effective nucleus–nucleus interaction potential between the two fragments can be expressed as follows:

$$V_{\rm cont}\left(Z_1,N_1,R_{\rm cont}\right) = V_{\rm C}\left(Z_1,N_1,R_{\rm cont}\right) + V_{\rm N}\left(Z_1,N_1,R_{\rm cont}\right). \tag{7}$$

The Coulomb potential is expressed as follows [77]:

$$V_{\rm C}\left(\mathbf{r},\theta_i\right) = \frac{Z_1Z_2e^2}{r} + \left(\frac{9}{20\pi}\right)^{1/2}\left(\frac{Z_1Z_2e^2}{r^3}\right)\times\sum_{i=1}^{2}R_i^2\beta_2^{(i)}P_2\left(\cos\theta_i\right) + \left(\frac{3}{7\pi}\right)\left(\frac{Z_1Z_2e^2}{r^3}\right)\times\sum_{i=1}^{2}R_i^2\left[\beta_2^{(i)}P_2\left(\cos\theta_i\right)\right]^2. \tag{8}$$

Here $\mathbf{r}$ denotes the centroid distance between the projectile and target nuclei, and R_i is the nuclear radius of fragment i. The nuclear potential can be written as [78]

$$V_{\rm N}(\mathbf{r},\theta) = C_0\left\{\frac{F_{\rm in}-F_{\rm ex}}{\rho_0}\left[\int\rho_1^2(\mathbf{r})\rho_2(\mathbf{r}-\mathbf{R})d\mathbf{r} + \int\rho_1(\mathbf{r})\rho_2^2(\mathbf{r}-\mathbf{R})d\mathbf{r}\right] + F_{\rm ex}\int\rho_1(\mathbf{r})\rho_2(\mathbf{r}-\mathbf{R})d\mathbf{r}\right\}, \tag{9}$$

with

$$F_{\rm in} = f_{\rm in} + f'_{\rm in}\frac{N_1-Z_1}{A_1}\frac{N_2-Z_2}{A_2},$$
$$F_{\rm ex} = f_{\rm ex} + f'_{\rm ex}\frac{N_1-Z_1}{A_1}\frac{N_2-Z_2}{A_2}.$$

where $C_0 = 300$ MeV fm^3, and the values of the amplitudes used in this study were taken from Ref. [79]; that is, $f_{\rm in} = 0.09$, $f_{\rm ex} = -2.59$, $f'_{\rm in} = 0.42$, and $f'_{\rm ex} = 0.5$. The mean nuclear density at the center of the composite system is $\rho_0 = 0.16$ fm^{-3}. The expressions $\rho_1(\mathbf{r})$ and $\rho_2(\mathbf{r}-\mathbf{R})$ represent the density distributions of the two nuclei, which are expressed in Woods–Saxon form.

The following equation expresses the production cross-section of the primary fragment with proton number Z and mass number A:

$$\sigma_{\rm pr}\left(Z_1,N_1,E_{\rm c.m.}\right) = \frac{\pi\hbar^2}{2\mu E_{\rm c.m.}}\sum_J(2J+1)\times\left[P\left(Z_1,N_1,E_1,t=\tau_{\rm int}\right)\right], \tag{10}$$

where P is regarded as the fragment distribution probability of nuclei with charge number Z and neutron number N, and $t = \tau_{\rm int}$ is the interaction time. The sequential statistical evaporation of excited fragments was calculated using the GEMINI++ code [80, 81]. The GEMINI++ code is an improved version of the GEMINI sequential decay code, capable of handling light particle evaporation, symmetric fission, and all potential binary-decay modes. To simulate nucleon and light particle evaporation, the Hauser–Feshbach formalism is applied. The Moretto formalism is used to model the emission of heavier fragments and asymmetric fission of heavy systems, while symmetric fission is predicted using the Bohr-Wheeler formalism, accounting for

structural evolution. GEMINI++ is commonly employed to treat both light particle evaporation and various binary-decay modes effectively.

3 Results and discussion

3.1 Comparison with experimental data

To inspect the reliability of DNS model in reproducing the transfer cross-sections of actinide nuclei, the production cross-sections with $Z = 95$–100 isotopes were investigated through the MNT reaction ^{129}Xe+^{248}Cm at an incident energy $E_{c.\,m.} = 513.10$ MeV.

As illustrated in Fig. 1, the cross-sections of target-like fragments (TLFs) as a function of the mass number are explicitly presented for the reaction ^{129}Xe+^{248}Cm. The black line denotes the distribution of final fragments obtained from the DNS model, while the solid circle represents the experimental data from Ref. [29]. The systematic trends observed in the theoretical results calculated using the DNS model closely align with the experimental data. The peak position of the theoretically calculated cross-section is in proximity to that of the experimental section. Additionally, the calculated isotopic distribution cross-sections exhibit a decrease with increasing proton numbers in the TLFs. For instance, the peak production cross-section for Am [see Fig. 1a] is two orders of magnitude larger than that of Fm (Fig. 1f). Furthermore, the nuclides investigated in these reactions are distributed in the transuranic region. This indicates that the combination of the DNS model and the GEMINI++ model can reliably extrapolate the multinucleon transfer reactions of actinide nuclei.

3.2 Charge equilibrium

To identify the two optimal colliding partners, collisions of the projectiles ^{124,129}Xe with the targets ^{248}Cm and ^{249}Cf were investigated for the production of trans-target nuclei at an incident energy of $E_{c.\,m.} = 1.1\ V_B$ (shown in Fig. 2). The V_B values for the ^{124}Xe+^{248}Cm, ^{124}Xe+^{249}Cf, and ^{129}Xe+^{249}Cf reactions are 497.4, 508.2, and 504.9 MeV.

From the ^{124}Xe+^{248}Cm (solid line), ^{124}Xe+^{249}Cf (dashed line), and ^{129}Xe+^{249}Cf (dash-dotted line) reactions, it can be seen that target nuclei with a smaller N/Z value are more favorable for producing neutron-deficient final fragments when the projectile is identical. In deep inelastic collisions, the trend of charge equilibration significantly influences the nucleon transfer process [82]. The N/Z ratios of ^{248}Cm and ^{249}Cf are 1.58 and 1.54, respectively. Compared to the ^{248}Cm

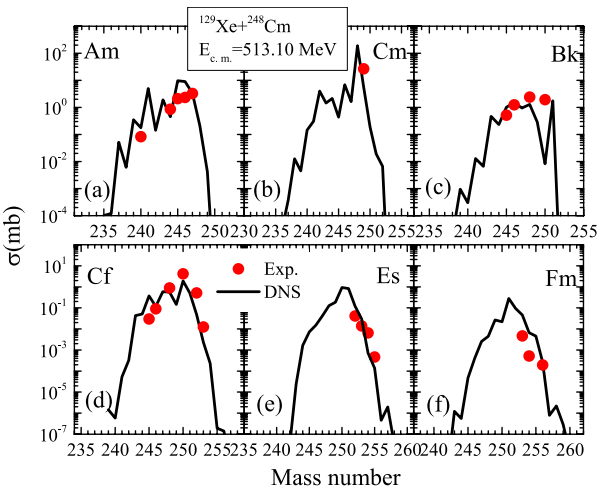

Fig. 1 (Color online) Target-like fragment (TLF) cross-sections depicted as a function of mass number in reaction ^{129}Xe+^{248}Cm at the incident energy 513.10 MeV. The solid lines denote the results obtained by the DNS and GEMINI++ models, while the solid circle represents the experimental data taken from Ref. [29]

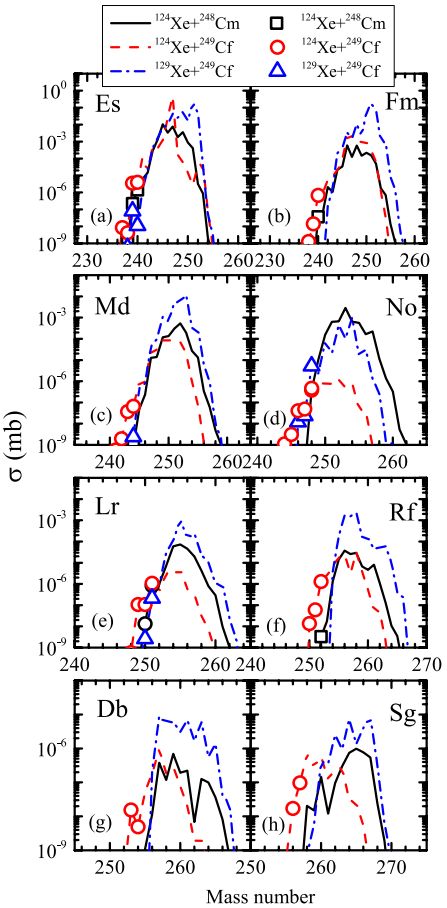

Fig. 2 (Color online) At an incident energy $E_{c.\,m.} = 1.1\ V_B$, the production of neutron-deficient trancalifornium nuclei with $Z = 99$–106 is investigated through the multinucleon transfer reactions, including ^{124}Xe+^{248}Cm (solid line), ^{124}Xe+^{249}Cf (dashed line), and ^{129}Xe+^{249}Cf (dash-dotted line). The open symbols indicate the new nuclide

target, ^{124}Xe (1.30) is more likely to transfer protons to the ^{249}Cf target.

When comparing the cross-sections generated by different Xe nuclei bombarding the same target nucleus ^{249}Cf in the MNT reactions, specifically the systems ^{124,129}Xe+^{249}Cf, neutron-deficient isotopes of einsteinium (Es), fermium (Fm), mendelevium (Md), nobelium (No), lawrencium (Lr), rutherfordium (Rf), dubnium (Db), and seaborgium (Sg) can be synthesized by transferring one to eight protons from the projectile to the target. The calculated results indicate that the cross-sections for the neutron-deficient isotopes with $Z = 99–106$ increase as the N/Z value for Xe isotopes decreases (with N/Z ratios are 1.30 and 1.38 for ^{124}Xe and ^{129}Xe, respectively). Thus, more neutron-deficient nuclei are favorable for producing unknown neutron-deficient isotopes. In summary, a reaction system with a low N/Z value, such as ^{124}Xe+^{249}Cf, represents the optimal combination of projectile and target for producing neutron-deficient isotopes with proton numbers $Z = 99–106$.

In principle, the MNT process can be described as a reaction occurring on the so-called potential energy surface (PES), where the dynamic evolution of a dinuclear system is viewed as an exchange process of independent particles between the projectile and target [50]. The PES of the fragments produced in the ^{124,129}Xe+^{249}Cf reactions as functions of Z_1 and N_1 are illustrated in Fig. 3, where open stars indicate the locations of injection points in the nucleus. The PES structure reveals that the fragments tend to form symmetric paths, characteristic of quasi-fission processes.

Figure 4 shows the driving potential of the ^{124,129}Xe+^{249}Cf reaction system, reaction system, corresponding to the minimum trajectory of the PES depicted in Fig. 3, where the valley shape of the driving potential is clearly evident. Open

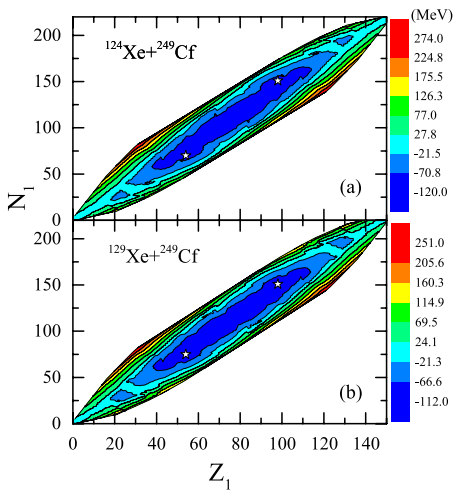

Fig. 3 (Color online) The PES as a function of Z_1 and N_1 of the fragment 1 in the reactions ^{124}Xe+^{249}Cf (**a**) and ^{129}Xe+^{249}Cf (**b**)

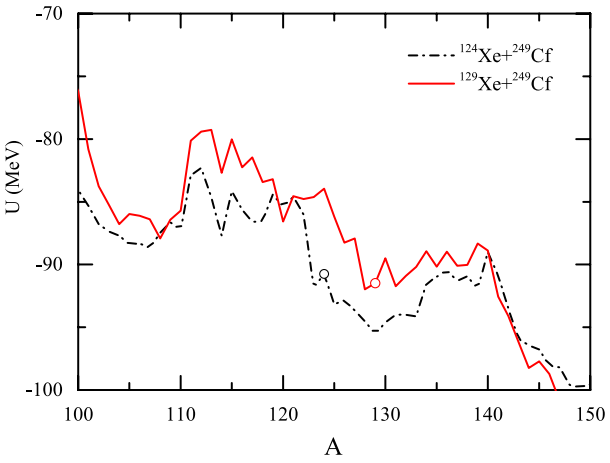

Fig. 4 (Color online) The driving potential of the ^{124,129}Xe+^{249}Cf reaction system corresponds to the minimum trajectory of the potential energy surface

circles in the figure denote the positions of the injection points for the projectile, while the dotted and dash-dotted lines represent the ^{124,129}Xe+^{249}Cf reaction systems. The position of ^{129}Xe is located within the valley of the driving potential, whereas the position of ^{124}Xe is situated at the opposite end. The transfer of a nucleon (proton or neutron) from the injection point to either side is influenced by the direction of the lower potential energy surface.

To explain the charge equilibration effect depicted in Fig. 2, the driving potential that must be overcome during nucleon transfer, defined as ($\Delta U = U(Z_1, N_1, Z_2, N_2) - U(Z_P, N_P, Z_T, N_T)$), is extracted and presented in Fig. 5a. In a pure proton pickup channel, the value of ΔU is positive and increases with the number of protons picked up, indicating that a significant amount of potential energy must be surpassed during proton pickup. Conversely, in the pure proton-stripping channel, ΔU remains positive but decreases slightly with an increasing number of stripped protons, making nucleon transfer in the proton-stripping channel easier due to the reduction in potential energy. Additionally, it is evident that the value of ΔU in the neutron pickup channel is smaller than that in the neutron-stripping channel. Consequently, the nucleus ^{124}Xe tends to gain neutrons over protons in the reaction ^{124}Xe+^{249}Cf. ΔU comprises $Q_{gg}(= M_P + M_T - M_{PLF} - M_{TLF})$ and a variation in the interaction potential energy.

Figure 5b shows the relationship between Q_{gg} during the nucleon transfer process and the number of nucleons transferred in the ^{124}Xe+^{249}Cf reaction (N_{tr}). It can be observed that the value of Q_{gg} in the pure proton-stripping channel is negative, and its absolute value increases with the number of stripped protons. This indicates that a considerable amount of energy must be absorbed in the pure proton-stripping channel. However, the formation probability in the neutron

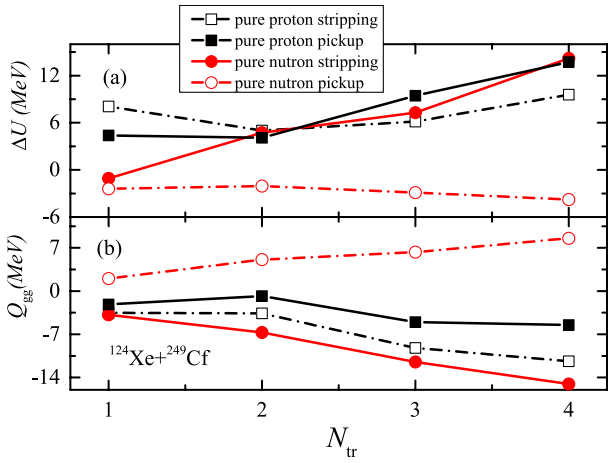

Fig. 5 (Color online) In ^{124}Xe+^{249}Cf reaction, the values of the driving potential to be overcome (**a**) and Q_{gg} (= $M_P + M_T - M_{PLF} - M_{TLF}$) values (**b**) during nucleon transfer as a function of the number of transferred nucleons (N_{tr}), M_P, M_T, M_{PLF}, and M_{TLF} are the masses of the nucleus, target nucleus, projectile-like fragments, and target-like fragments, respectively

pickup channel is significantly higher than that in the proton pickup channel. From this, the following conclusions can be drawn: The MNT reaction within neutron-deficient beams is advantageous for accessing neutron-deficient isotopes along the trans-target region.

3.3 Incident energy dependence

The incident energy plays a critical role in MNT reactions, as shown in Fig. 6, which presents the production cross-sections for Es, Md, Lr, and Db isotopes in the ^{124}Xe+^{249}Cf reaction at different incident energies. The solid, dashed, and dash-dotted lines denote 1.05 V_B, 1.10 V_B, and 1.20 V_B, respectively.

It is clear that the primary fragment cross-sections are significantly influenced by the incident energy, with higher energies leading to increased cross-sections.

For actinide nuclei with an abundance of neutrons, the final fragment cross-sections also depend heavily on the incident energy, due to the higher likelihood of fission. Compared to the primary cross-section, the mass region of the final cross-section becomes narrower after the de-excitation process. Additionally, a double-peak phenomenon is observed in both the primary and final isotopic cross-sections for the Es isotopes. This effect is mainly attributed to the neutron sub-shell influence identified at $N = 152$ [83]. Comparing these three different incident energies reveals that the production cross-sections on the neutron-deficient side are not sensitive to the incident energy variations. To minimize the chance of fission, the incident energy was set

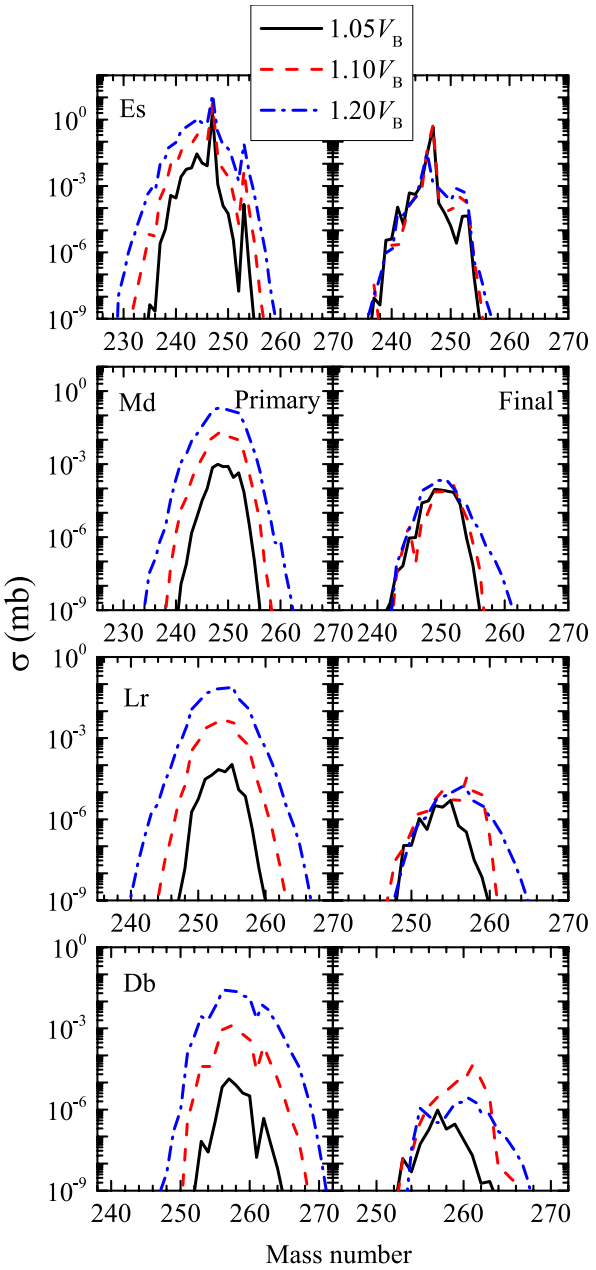

Fig. 6 (Color online) Production cross-sections for Es, Md, Lr, and Db isotopes in the ^{124}Xe+^{249}Cf reaction at various incident energies. The solid, dashed, and dash-dotted lines indicate 1.05, 1.10, and 1.20 V_B, respectively

to 1.05 V_B (533.64 MeV), which is optimal for producing new neutron-deficient nuclei.

In the DNS model, the interaction time directly affects the probability distribution and excitation energy of fragments during the transfer process. Figure 7 illustrates the evolution of interaction time with "effective" angular momentum (where "effective" refers to the distance at which the target interacts with the projectile) at different energies in the ^{124}Xe+^{249}Cf reaction, where the dashed-dotted, solid,

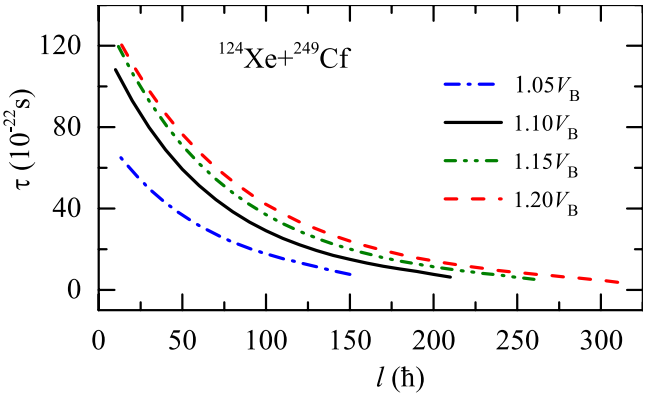

Fig. 7 (Color online) Evolution of the interaction time with angular momentum under different energies in the ^{124}Xe+^{249}Cf reaction, where the dash-dotted, solid, dash-dot-dotted, and dashed lines indicate 1.05, 1.10, 1.15, and 1.20 V_B, respectively

dashed-dotted, and dashed lines indicate 1.05, 1.10, 1.15, and 1.20 V_B, respectively. Here, the reaction time is calculated by deflection function [84].

As the incident energy increases, the range of "effective" angular momentum also expands, while the rate of change in "effective" angular momentum diminishes with higher energy. For the energy differences $E_{c.\,m.} = 1.05$, 1.10, 1.15, and 1.20 V_B, it is observed that interaction time decreases as "effective" angular momentum increases. Simultaneously, the range of interaction time increases with the rising incident energy. This occurs because, with higher incident energy, the internal excitation energy dissipated into the dinuclear system increases, leading to a greater interaction distance and extended evolution time between the two nuclei.

4 Landscape of the neutron-deficient transcalifornium nuclei

Charge balance and energy effects were also examined, indicating that the ^{124}Xe+^{249}Cf reaction is most favorable for producing new neutron-deficient nuclei at an incident energy of 1.05 V_B. Beam ^{124}Xe has an intensity of 6×10^9 ions/s [85]. The thickness of ^{249}Cf target was 0.34 mg/cm^2 in Dubna [86]. In Fig. 8, the production cross-sections for several unknown neutron-deficient isotopes with $Z = 99–106$ in the ^{124}Xe+^{249}Cf reaction are presented, along with their distributions in the nuclide diagram. This highlights the potential for detecting these neutron-deficient isotopes through time- and position-correlated α-decay chains, which is a common experimental approach [87, 88]. From the data presented, a total of 25 new nuclei are predicted to be produced. The DNS model provides the following cross-section predictions for specific isotopes: $^{237–240}$Es of 0.009, 0.004, 3.504, and 3.980 nb; $^{238–240}$Fm of 0.001, 0.014, and 0.678 nb; $^{242–244}$Md of 0.002, 0.036, and 0.066 nb cross-sections for $^{244–248}$No are 0.001, 0.003, 0.040, 0.049, and 0.468 nb; cross-sections for $^{249–251}$Lr are 0.107, 0.108, and 1.080 pb; cross-sections for $^{250–252}$Rf are 0.013, 0.060, and 1.290 nb; ^{253,254}Db with cross-sections of 0.015 and 0.005 nb; and ^{256,257}Sg with cross-sections of 0.017 and 0.097 nb, respectively.

5 Summary and outlook

The properties of neutron-deficient heavy isotopes are essential for exploring shell evolution and the proton drip line. The synthesis of neutron-deficient isotopes within the range of $Z = 99–106$ was investigated through MNT reactions, utilizing the combination of the DNS model and GEMINI++. A comparison of the calculated results with experimental

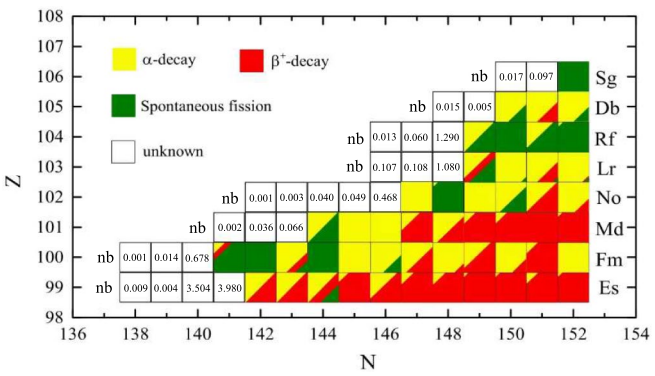

Fig. 8 (Color online) Landscape of nuclide diagrams with $Z = 99–106$ isotopes produced in the ^{124}Xe+^{249}Cf reaction. Yellow, red, and green squares indicate α-decay, β^+-decay, and spontaneous fission, respectively, and blank squares represent the predicted new nuclei

data from the reaction ^{129}Xe+^{248}Cm at an incident energy of 513.10 MeV demonstrates that the DNS model, in conjunction with the GEMINI++ code, effectively describes the MNT reactions in heavy-mass systems. To produce exotic neutron-deficient transcalifornium nuclei, MNT reactions involving ^{124}Xe+^{248}Cm, ^{124}Xe+^{249}Cf, and ^{129}Xe+^{249}Cf were studied. Owing to the competition between the sub-shell effect at $N = 152$ and charge equilibrium, the cross-sections of neutron-deficient trancalifornium nuclei are enhanced. Along the pure neutron and proton-stripping channels, it is evident that the pure neutron-stripping channel exhibits a larger absolute value of Q_{gg}, indicating that transferring neutrons from the projectile to the target is more challenging than transferring protons. Additionally, the effect of incident energy on the yield of TLFs in the ^{124}Xe+^{249}Cf reaction was also explored. The optimal incident energy for producing neutron-deficient isotopes, with $Z = 99$–106, was identified as $E_{\mathrm{c.\,m.}} = 533.64$ MeV.

Author contributions All authors contributed to the study conception and design. Material preparation, data collection, and analysis were performed by Na Tang, Si-Ying Ma, Rong An, Jing-Jing Li, and Feng-Shou Zhang. The first draft of the manuscript was written by Na Tang, and all authors commented on the previous versions of the manuscript. All authors read and approved the final manuscript.

Data availability The data that support the findings of this study are openly available in Science Data Bank at https://cstr.cn/31253.11.sciencedb.j00186.00434 and https://www.doi.org/10.57760/sciencedb.j00186.00434.

Declarations

Conflict of interest The authors declare that they have no conflict of interest.

References

1. S. Hofmann, G. Münzenberg, The discovery of the heaviest elements. Rev. Mod. Phys.**72**, 733 (2000). https://doi.org/10.1103/RevModPhys.72.733
2. Y.T. Oganessian, V.K. Utyonkov, Super-heavy element research. Rep. Prog. Phys. **78**, 036301 (2015). https://doi.org/10.1088/0034-4885/78/3/036301
3. Y. Oganessian, Isospin asymmetry in nuclei and neutron stars. Phys. Rept. **411**, 325 (2005). https://doi.org/10.1088/0954-3899/34/4/R01
4. G.G. Adamian, N.V. Antonenko, A. Diaz-Torres et al., How to extend the chart of nuclides? Eur Phys J. A **56**, 1 (2020). https://doi.org/10.1140/epja/s10050-020-00046-7
5. J. F. Xu, C. J. Xia, Z. Y. Lu et al., How to approach the island of stability: reactions using multinucleon transfer or radioactive neutron-rich beams? Phys. Lett. B **829**, 137113 (2022). https://doi.org/10.1016/j.physletb.2022.137113
6. M. H. Zhang, Y. H. Zhang, J. J. Li et al. (2023) Progress in transport models of heavy-ion collisions for the synthesis of superheavy nuclei. Nucl. Tech. (in Chinese) **46**: 080014 https://doi.org/10.11889/j.0253-3219.2023.hjs.46.080014
7. Y.Q. Xin, N.N. Ma, J.G. Deng et al., Properties of Z=114 superheavy nuclei. Nucl. Sci. Tech. **32**, 55 (2021). https://doi.org/10.1007/s41365-021-00899-7
8. C. A. Laue, K. E. Gregorich, R. Sudowe et al., New plutonium isotope: ^{231}Pu. Phys. Rev. C **59**, 3086 (1999). https://doi.org/10.1103/PhysRevC.59.3086
9. L. Ma, Z. Y. Zhang, Z. G. Gan et al., α-decay properties of the new isotope ^{216}U. Phys. Rev. C **91**, 051302 (2015). https://doi.org/10.1103/PhysRevC.91.051302
10. H. B. Yang, L. Ma, Z. Y. Zhang et al., Alpha decay properties of the semi-magic nucleus ^{219}Np. Phys. Lett. B **777**, 212 (2018). https://doi.org/10.1016/j.physletb.2017.12.017
11. X.B. Yu, L. Zhu, Z.H. Wu et al., Predictions for production of superheavy nuclei with $Z = 105 - 112$ in hot fusion reactions. Nucl. Sci. Tech. **29**, 154 (2018). https://doi.org/10.1007/s41365-018-0501-2
12. G. Münzenberg, S. Hofmann, F.P. Heßberger et al., Identification of element 107 by α correlation chains. Z. Phys. A **309**, 89 (1982). https://doi.org/10.1007/BF01412623
13. G. Münzenberg, P. Armbruster, F.P. Heßberger et al., Observation of one correlated?-decay in the reaction ^{58}Fe on^{209}Bi. Z. Phys. A **309**, 89 (1982). https://doi.org/10.1007/BF01420157
14. S. Hofmann, V. Ninov, F.P. Heßberger et al., The new element 111. Z. Phys. A **350**, 281 (1995). https://doi.org/10.1007/BF01291182
15. G. Münzenberg, P. Armbruster, H. Folger et al., The identification of element 108. Z. Phys. A **317**, 235 (1984). https://doi.org/10.1007/BF01421260
16. S. Hofmann, V. Ninov, F. P. Heßberger et al., Production and decay of ^{269}110. Z. Phys. A **350**, 277 (1995). https://doi.org/10.1007/BF01291181
17. J. L. Pore, J. M. Gates, R. Orford et al, Identification of the new isotope ^{244}Md. Phys. Rev. Lett. **124**, 252502 (2020). https://doi.org/10.1103/PhysRevLett.124.252502
18. V. K. Utyonkov, N. T. Brewer, Yu. Ts. Oganessian et al., Experiments on the synthesis of superheavy nuclei ^{284}Fl and ^{285}Fl in the ^{239,240}Pu +^{48}Ca reactions. Phys. Rev. C **92**, 034609(2015). https://doi.org/10.1103/PhysRevC.92.034609
19. M. D. Sun, Z. Liu, T. H. Huang et al., New short-lived isotope ^{223}Np and the absence of the $Z = 92$ subshell closure near $N = 126$. Phys. Lett. B **771**, 303 (2017). https://doi.org/10.1016/j.physletb.2017.03.074
20. Z. Y. Zhang, H. B.Yang, M. H. Huang et al., New α-Emitting Isotope ^{214}U and Abnormal Enhancement of α-Particle Clustering in Lightest Uranium Isotopes. Phys. Rev. Lett. **126**, 152502 (2021). https://doi.org/10.1103/PhysRevLett.126.152502
21. J. Khuyagbaatar, H. Brand, R. A. Cantemir et al., Spontaneous fission instability of the neutron-deficient No and Rf isotopes: the new isotope ^{249}No. Phys. Rev. C **104**, L031303 (2021). https://doi.org/10.1103/PhysRevC.104.L031303
22. M.H. Zhang, Y. Zou, M.C. Wang et al., Possibility of reaching the predicted center of the "island of stability'' via the radioactive beam-induced fusion reactions. Nucl. Sci. Tech. **35**, 161 (2024). https://doi.org/10.1007/s41365-024-01542-x
23. S.H. Zhu, T.L. Zhao, X.J. Bao et al., Systematic study of the synthesis of heavy and superheavy nuclei in ^{48}Ca-induced fusion-evaporation reactions. Nucl. Sci. Tech. **35**, 124 (2024). https://doi.org/10.1007/s41365-024-01483-5
24. P.H. Chen, C. Geng, X.H. Zeng et al., Influence of entrance channel on production cross sections of exotic actinides in multinucleon transfer reactions. Phys. Rev. C **106**, 054601 (2022). https://doi.org/10.1103/PhysRevC.106.054601
25. M. Barbui, K. Hagel, J.B. Natowitz et al., Search for Heavy and Superheavy systems in ^{197}Au+^{232}Th Collisions near the

Coulomb Barrier. J. Phys. **312**, 082012 (2011). https://doi.org/10.1088/1742-6596/312/8/082012
26. Z. Majka, M. Barbui, F. Becchetti et al., Experimental search for super and hyper heavy nuclei at cyclotron Institute Texas A & M University. Acta Phys. Polonica. B **45**, 279 (2014). https://doi.org/10.5506/APhysPolB.45.279
27. A. Wieloch, M. Adamczyk, M. Barbui et al., A novel approach to the island of stability of super-heavy elements search. EPJ Web Conf. **117**, 01003 (2016). https://doi.org/10.1051/epjconf/201611701003
28. K.J. Moody, D. Lee, R.B. Welch et al., Actinide production in reactions of heavy ions with ^{248}Cm. Phys. Rev. C **33**, 1315 (1986). https://doi.org/10.1103/PhysRevC.33.1315
29. R. B. Welch, K. J. Moody, K. E. Gregorich et al., Dependence of actinide production on the mass number of the projectile: Xe + ^{248}Cm. Phys. Rev. C **35**, 204 (1987). https://doi.org/10.1103/PhysRevC.35.204
30. P. Glässel, D. V. Harrach, Y. Civelekoglu et al., Three-particle exclusive measurements of the reactions ^{238}U + ^{238}U and ^{238}U + ^{248}Cm. Phys. Rev. Lett. **43**, 1483 (1979). https://doi.org/10.1103/PhysRevLett.43.1483
31. A. G. Artukh, G. F. Gridnev, V. L. Mikheev et al., Transfer reactions in the interaction of ^{40}Ar with ^{232}Th. Nucl. Phys. A **215**, 91 (1973). https://doi.org/10.1016/0375-9474(73)90104-8
32. A. G. Artukh, G. F. Gridnev, V. L. Mikheev et al., New isotopes ^{22}O, ^{20}N and ^{18}C produced in transfer reactions with heavy ions. Nucl. Phys. A **137**, 348 (1969). https://doi.org/10.1016/0375-9474(69)90114-6
33. A. G. Artukh, G. F. Gridnev , V. L. Mikheev et al., Multinucleon transfer reactions in the ^{232}Th+ ^{22}Ne system . Nucl. Phys. A **211**, 299 (1973). https://doi.org/10.1016/0375-9474(73)90721-5
34. A. G. Artukh, V. V. Avdeichikov, G. F. Gridnev et al., New isotopes ^{29,30}Mg, ^{31,32,33}Al, ^{31,32,33}Si, ^{35,36,37,38}P, ^{39,40}S and ^{41,42}Cl produced in bombardment of a ^{232}Th target with 290 MeV ^{40}Ar ions. Nucl. Phys. A **176**, 284 (1971). https://doi.org/10.1103/PhysRevLett.129.042501
35. L. Zhu, Possibilities of producing superheavy nuclei in multinucleon transfer reactions based on radioactive targets . Chin. Phys. C **43**, 124103 (2019). https://doi.org/10.1088/1674-1137/43/12/124103
36. Y. H. Zhang, J. J. Li, N. Tang et al., Production cross sections of new neutron-rich isotopes with $Z = 92 - 106$ in the multinucleon transfer reaction ^{197}Au + ^{232}Th. Phys. Rev. C **107**, 024604 (2023). https://doi.org/10.1103/PhysRevC.107.024604
37. J. J. Li, N. Tang, Y. H. Zhang et al., Theoretical study on the production of neutron-rich transuranium nuclei with radioactive beams in multinucleon transfer reactions. Phys. Rev. C **106**, 014606 (2023). https://doi.org/10.1103/PhysRevC.106.014606
38. H.M. Devaraja, S. Heinz, O. Beliuskina et al., IObservation of new neutron-deficient isotopes with Z≥92 in multinucleon transfer reactions. Phys. Lett. B **748**, 199 (2015). https://doi.org/10.1016/j.physletb.2015.07.006
39. T. Niwase, Y. X. Watanabe, Y. Hirayama et al., Discovery of new isotope ^{241}U and systematic high-precision atomic mass measurements of neutron-rich Pa-Pu nuclei produced via multinucleon transfer reactions. Phys. Rev. Lett. **130**, 132502 (2023). https://doi.org/10.1103/PhysRevLett.130.132502
40. A. Winther, Grazing reactions in collisions between heavy nuclei. Nucl. Phys. A **572**, 191 (1994). https://doi.org/10.1016/0375-9474(94)90430-8
41. A. Winther, Dissipation, polarization and fluctuation in grazing heavy-ion collisions and the boundary to the chaotic regime. Nucl. Phys. A **594**, 203 (1995). https://doi.org/10.1016/0375-9474(95)00374-A
42. R. Yanez, W. Loveland, Predicting the production of neutron-rich heavy nuclei in multinucleon transfer reactions using a semi-classical model including evaporation and fission competition, GRAZING-F. Phys. Rev. C **91**, 044608 (2015). https://doi.org/10.1103/PhysRevC.91.044608
43. V. V. Volkov, Deep inelastic transfer reactions –The new type of reactions between complex nuclei. Phys. Rept. **44**, 93 (1978). https://doi.org/10.1016/0370-1573(78)90200-4
44. G.G. Adamian, N.V. Antonenko, D. Lacroix, Production of neutron-rich Ca, Sn, and Xe isotopes in transfer-type reactions with radioactive beams. Phys. Rev. C **82**, 064611 (2010). https://doi.org/10.1103/PhysRevC.82.064611
45. Z.Q. Feng, G.M. Jin, J.Q. Li, Production of heavy isotopes in transfer reactions by collisions of ^{238}U + ^{238}U. Phys. Rev. C **80**, 067601 (2009). https://doi.org/10.1103/PhysRevC.80.067601
46. M.H. Mun, K. Kwak, G.G. Adamian et al., Possible production of neutron-rich No isotopes. Phys. Rev. C **101**, 044602 (2020). https://doi.org/10.1103/PhysRevC.101.044602
47. N. Tang, X.R. Zhang, J.J. Li et al., Production of unknown neutron-rich isotopes with $Z = 99 - 102$ in multinucleon transfer reactions near the Coulomb barrier. Phys. Rev. C **106**, 034601 (2022). https://doi.org/10.1103/PhysRevC.106.034601
48. T.L. Zhao, X.J. Bao, H.F. Zhang et al., Exploring the optimal way to produce $Z = 100 - 106$ neutron-rich nuclei. Phys. Rev. C **108**, 024602 (2023). https://doi.org/10.1103/PhysRevC.108.024602
49. S. Y. Xu, Z. Q. Feng, Cluster emission in massive transfer reactions based on dinuclear system model. Nucl. Tech. (in Chinese) **46**, 030501 (2023). https://doi.org/10.11889/j.0253-3219.2023.hjs.46.030501
50. Z.H. Liao, L. Zhu, J. Su et al., Dynamics of charge equilibration and effects on producing neutron-rich isotopes around $N = 126$ in multinucleon transfer reactions. Phys. Rev. C **107**, 014614 (2023). https://doi.org/10.1103/PhysRevC.107.014614
51. V. Zagrebaev, W. Greine, Low-energy collisions of heavy nuclei: dynamics of sticking, mass transfer and fusion. J. Phys. G **34**, 1 (2006). https://doi.org/10.1088/0954-3899/34/1/001
52. V. I. Zagrebaev, W. Greiner (2011) Production of heavy and superheavy neutron-rich nuclei in transfer reactions. Phys. Rev. C **83**, 044618. https://doi.org/10.1103/PhysRevC.83.044618
53. V. Zagrebaev, W. Greiner, New way for the production of heavy neutron-rich nuclei. J. Phys. G **35**, 125103 (2008). https://doi.org/10.1088/0954-3899/35/12/125103
54. V. Zagrebaev, W. Greiner, Synthesis of superheavy nuclei: A search for new production reactions. Phys. Rev. C **78**, 034610 (2008). https://doi.org/10.1103/PhysRevC.78.034610
55. V. V. Saiko, A.V. Karpov, IAnalysis of multinucleon transfer reactions with spherical and statically deformed nuclei using a Langevin-type approach. Phys. Rev. C **99**, 014613 (2019). https://doi.org/10.1103/PhysRevC.99.014613
56. V. Zagrebaev, W. Greiner, Production of new heavy isotopes in low-energy multinucleon transfer reactions. Phys. Rev. C **101**, 122701 (2008). https://doi.org/10.1103/PhysRevLett.101.122701
57. K. Zhao, Z.X. Li, N. Wang et al., Production mechanism of neutron-rich transuranium nuclei in ^{238}U + ^{238}U collisions at near-barrier energies. Phys. Rev. C **92**, 024613 (2015). https://doi.org/10.1103/PhysRevC.92.024613
58. C. Li, P.W. Wen, J.J. Li et al., Production mechanism of new neutron-rich heavy nuclei in the ^{136}Xe + ^{198}Pt reaction. Phys. Lett. B **776**, 278 (2018). https://doi.org/10.1016/j.physletb.2017.11.060
59. K. Zhao, Z. Liu, F.S. Zhang et al., Production of neutron-rich N=126 nuclei in multinucleon transfer reactions: comparison between ^{136}Xe + ^{198}Pt and ^{238}U +^{198}Pt reactions. Phys. Lett. B **815**, 136101 (2021). https://doi.org/10.1016/j.physletb.2021.13610

60. C. Li, F. Zhang, J.J. Li et al., Multinucleon transfer in the ^{136}Xe + ^{208} Pb reaction. Phys. Rev. C **93**, 014618 (2016). https://doi.org/10.1103/PhysRevC.93.014618
61. C. Li, J. L. Tian, F. S. Zhang, Production mechanism of the neutron-rich nuclei in multinucleon transfer reactions: A reaction time scale analysis in energy dissipation process. Phys. Lett. B **809**, 135697 (2020). https://doi.org/10.1016/j.physletb.2020.135697
62. K. Godbey, C. Simenel, A.S. Umar, Microscopic predictions for the production of neutron-rich nuclei in the reaction ^{176}Yb + ^{176}Yb. Phys. Rev. C **101**, 034602 (2020). https://doi.org/10.1103/PhysRevC.101.034602
63. Z.J. Wu, L. Guo, Z. Liu et al. , Production of proton-rich nuclei in the vicinity of ^{100}Sn via multinucleon transfer reactions. Phys. Lett. B **825**, 136886 (2022). https://doi.org/10.1016/j.physletb.2022.136886
64. L. Guo, C. Simenel, L. Shi et al., The role of tensor force in heavy-ion fusion dynamics. Phys. Lett. B **782**, 401 (2018). https://doi.org/10.1016/j.physletb.2018.05.066
65. X.J. Bao, S.Q. Guo, P.H. Chen, Production of new neutron-rich isotopes with $92 \leq Z \leq 100$ in multinucleon transfer reactions. Phys. Rev. C **105**, 024610 (2022). https://doi.org/10.1103/PhysRevC.105.024610
66. Z.J. Wu, L. Guo, Production of proton-rich actinide nuclei in the multinucleon transfer reaction ^{58}Ni + ^{232}Th. Sci. China. Phys. Mech. Astron. **63**, 242021 (2020). https://doi.org/10.1007/s11433-019-1484-0
67. Z.H. Liao, L. Zhu, Z.P. Gao et al., Optimal detection angles for producing $N = 126$ neutron-rich isotones in multinucleon transfer reactions. Phys. Rev. Res. **5**, L022021 (2023). https://doi.org/10.1103/PhysRevResearch.5.L022021
68. P. H. Chen, F. Niu, Z. Q. Feng, Production mechanism of proton-rich actinide isotopes in fusion reactions and via multinucleon transfer processes. Phys. Rev. C **102**, 014621 (2020). https://doi.org/10.1103/PhysRevC.102.014621
69. L. Zhu, F. S. Zhang, P. W. Wen et al., Production of neutron-rich nuclei with $Z = 60 - 73$ in reactions induced by Xe isotopes. Phys. Rev. C **96**, 024606 (2017). https://doi.org/10.1103/PhysRevC.96.024606
70. S. Ayik, B. Schürmann, W. Nörenberg, Microscopic transport theory of heavy-ion collisions. Z. Phys. A **277**, 299 (1976). https://doi.org/10.1007/bf01415605
71. J. Q. Li, X. T. Tang, G. Wolschin, Anticorrelated angular-momentum distributions in heavy-ion collisions. Phys. Lett. B **105**, 107 (1981). https://doi.org/10.1016/0370-2693(81)91000-5
72. J.J. Li, G. Zhang, X.R. Zhang et al., Production of unknown neutron−rich transuranium isotopes $^{245-249}$Np, $^{248-251}$Pu, $^{248-254}$Am, and $^{252-254}$Cm in multinucleon transfer reactions. J. Phys. G **49**, 025106 (2022). https://doi.org/10.1088/1361-6471/ac44ad
73. X. R. Zhang, G. Zhang, J. J. Li et al., Effects of nucleus orientation on transfer process and production of unknown neutron-rich isotopes with $Z = 62 - -75$ in ^{204}Hg + ^{232}Th based on the dinuclear system model. Phys. Rev. C **103**, 024608 (2021). https://doi.org/10.1103/PhysRevC.103.024608
74. G. G. Adamian, N. V. Antonenko, W. Scheid, Model of competition between fusion and quasifission in reactions with heavy nuclei. Nucl. Phys. A **618**, 176 (1997). https://doi.org/10.1016/S0375-9474(97)88172-9
75. G. G. Adamian, N. V. Antonenko, W. Scheid et al., Fusion cross sections for superheavy nuclei in the dinuclear system concept. Nucl. Phys. A **633**, 409 (1998). https://doi.org/10.1016/S0375-9474(98)00124-9
76. P. Möller, J. R. Nix, W. D. Myers, Nuclear ground-state masses and deformations. At. Data Nucl. Data Tables **59**, 185 (1995). https://doi.org/10.1006/adnd.1995.1002
77. C. Y Wong, Interaction barrier in charged-particle nuclear reactions. Phys. Rev. Lett. **31**, 766 (1973). https://doi.org/10.1103/PhysRevLett.31.766
78. G.G. Adamian, N.V. Antonenko, W. Scheid et al., Characteristics of quasifission products within the dinuclear system model. Phys. Rev. C **68**, 034601(2003). https://doi.org/10.1103/PhysRevC.68.034601
79. A. B. Migdal, Theory of finite Fermi systems and applications to atomic nuclei. Theory of finite Fermi systems and applications to atomic nuclei (Interscience, New York) (1967). https://doi.org/10.1119/1.1975177
80. R. J. Charity, Systematic description of evaporation spectra for light and heavy compound nuclei. Phys. Rev. C **82**, 014610 (2010). https://doi.org/10.1103/PhysRevC.82.014610
81. D. Mancusi, R.J. Charity, J. Cugnon, Unified description of fission in fusion and spallation reactions. Phys. Rev. C **82**, 044610 (2010). https://doi.org/10.1103/PhysRevC.82.044610
82. L. Zhu, J. Su, W. J. Xie et al., Theoretical study on production of heavy neutron-rich isotopes around the N=126 shell closure in radioactive beam induced transfer reactions. Phys. Lett. B **767**,437 (2017). https://doi.org/10.1016/j.physletb.2017.01.082
83. A. Ghiorso, S.G. Thompson, G.H. Higgins et al., Evidence for Subshell at $N = 152$. Phys. Rev. **95**, 293 (1954). https://doi.org/10.1103/PhysRev.95.293
84. G. Wolschin, W. Norenberg, Analysis of relaxation phenomena in heavy-ion collisions. Z. Phys. A **284**, 209 (1978). https://doi.org/10.1007/BF01411331
85. G. Rainovski, N. Pietralla, T. Ahn et al., How close to the O(6) symmetry is the nucleus ^{124}Xe? Phys. Lett. B **683**, 11 (2010). https://doi.org/10.1016/j.physletb.2009.12.007
86. N. T. Brewer, V. K. Utyonkov, K. P. Rykaczewski et al., Search for the heaviest atomic nuclei among the products from reactions of mixed-Cf with a ^{48}Ca beam. Phys. Rev. C **98**, 024317 (2018). https://doi.org/10.1103/PhysRevC.98.024317
87. S. Hofmann, S. Dmitriev, C. Fahlander et al., On the discovery of new elements (IUPAC/IUPAP Provisional Report): provisional Report of the 2017 Joint Working Group of IUPAC and IUPAP. Pure Appl. Chem. **90**, 1773 (2018). https://doi.org/10.1515/pac-2018-0918
88. Z. Wang, Z.Z. Ren, Predictions of the decay properties of the superheavy nuclei ^{293,294}119 and ^{294,295}120. Nucl. Tech. (in Chinese) **46**, 080011 (2023). https://doi.org/10.11889/j.0253-3219.2023.hjs.46.080011